Spin and charge dynamics for the one-dimensional t-J model

J. Deisz
Department of Physics, The Ohio State University, Columbus, Ohio 43210
*and Department of Physics, Montana State University, Bozeman, Montana 59717**

K.-H. Luk
Department of Physics, The Ohio State University, Columbus, Ohio 43210

M. Jarrell
Department of Physics, The Ohio State University, Columbus, Ohio 43210
*and Department of Physics, University of Cincinnati, Cincinnati, Ohio 45221**

D. L. Cox
Department of Physics, The Ohio State University, Columbus, Ohio 43210
(Received 1 April 1991; revised manuscript received 29 January 1992)

The dynamic spin and charge correlation functions are computed for the one-dimensional t-J model with use of world-line quantum Monte Carlo and the maximum-entropy method. By comparing our results with exactly known limits, we are able to discern the power and limitations of this method. The spin excitation spectrum shows gapless spin excitations for $q=2k_F$ when $J\leq 2t$ and for $q=\pi$ when $J>3.25t$ where phase separation occurs. Also, intermediate values of J/t show no spin gap for the large electron filling ($\rho_0=0.75$) considered here. For $J\leq 2t$, the charge correlations are dominated at high frequencies by excitations which are related to the particle-hole excitations found for $J=0$, but a low-frequency mode appears at finite values of J, which is likely related to the binding of electron pairs.

I. INTRODUCTION

The t-J model described in one dimension by

$$H=-t\sum_{i,\sigma}P(c^{\dagger}_{i,\sigma}c_{i+1,\sigma}+c^{\dagger}_{i+1,\sigma}c_{i,\sigma})P$$
$$+J\sum_i \mathbf{S}_i\cdot\mathbf{S}_{i+1}-n_in_{i+1}/4\ , \tag{1}$$

where P projects out states containing doubly occupied sites, has been of considerable interest since Anderson[1] and Zhang and Rice[2] suggested that the two-dimensional t-J model may be for describing the low-energy electronic properties of high-T_c superconductors. The one-dimensional t-J model is also of interest for describing strong correlations in one-dimensional conductors. For one dimension exact Bethe-ansatz results have been found for $J\ll t$ (Ref. 3) and $J=2t$.[4] However, the complexity of the Bethe ansatz wave functions prevent many quantities of interest, such as the dynamic spin and charge susceptibilities, from being obtained. Thus numerical studies for all finite values of J/t are of interest.

In this paper we report results for the spin and charge spectra obtained with the world-line Monte Carlo[5] and maximum-entropy methods.[6] The combination of these methods, which is most accurate at low frequencies, has been shown to describe the qualitative difference between the excitation spectra of $S=\frac{1}{2}$ and $S=1$ antiferromagnetic Heisenberg chains and provides a quantitatively accurate vaue for the Haldane gap for $S=1$.[7] With this technique we obtain approximate, but nonperturbative, results for the dynamic spin and charge structure factors

$$S_{nn}(q,\omega)=\frac{\pi}{Z}\sum_{R,\sigma,\sigma'}e^{-iqR}\sum_{m,n}e^{-\beta E_m}\langle m|c^{\dagger}_{R,\sigma}c_{R,\sigma}|n\rangle\langle n|c^{\dagger}_{0,\sigma'}c_{0,\sigma'}|m\rangle\delta(\omega-(E_n-E_m))\ , \tag{2}$$

$$S_{zz}(q,\omega)=\frac{\pi}{4Z}\sum_{R,\sigma,\sigma'}e^{-iqR}\sum_{m,n}e^{-\beta E_m}\langle m|\sigma c^{\dagger}_{R,\sigma}c_{R,\sigma}|n\rangle\langle n|\sigma' c^{\dagger}_{0,\sigma'}c_{0,\sigma'}|m\rangle\delta(\omega-(E_n-E_m))\ , \tag{3}$$

which are related to the corresponding dynamic susceptibilities by

$$\chi''(q,\omega)=(1-e^{-\beta\omega})S(q,\omega)\ . \tag{4}$$

The dynamic structure factors describe many low-lying excitations. $S_{zz}(q,\omega)$ probes excitations where the total spin changes by at most one unit, for example, spin waves in an ordered magnetic system. $S_{nn}(q,\omega)$ probes excitations with changes in the charge degrees of freedom, for example, particle-hole excitations or plasmons in a Coulomb gas. Two features that appear in these results for the dynamic structure factors of the one-dimensional

t-J model are a sharp charge excitation when J/t becomes finite and zero-frequency spin excitations for all values of J/t at the large electron filling ρ_0 considered here.

Before describing these and other results we briefly review previous work relating to the dynamics of the one-dimensional t-J model. Exact and numerical results suggest that the spin and charge correlation functions are Hubbard-like when $J \leq 2t$. For the Bethe-ansatz soluble $U>0$ Hubbard model, the asymptotic properties of the equal-time correlation functions suggest gapless spin excitations are found with momentum $2k_F=\pi\rho_0$ and gapless charge excitations with momenta $2k_F$ and $4k_F$.[8] Because the $U \gg t$ Hubbard model is equivalent to the t-J model for $J \ll t$ these properties are expected to be found for the t-J model when $J \ll t$. the $J=2t$ Bethe-ansatz solution shares these same features suggesting similar behavior for all $J \leq 2t$. Monte Carlo simulations,[9] variational theory,[10] and finite-size scaling[11] suggest that indeed there are no qualitative changes in the static properties of the t-J model as a function of J/t for $J \leq 2t$.

Few exact results are available for $J>2t$. Monte Carlo results due to Imada[12] and Assaad and Würtz[9] and variational results due to Hellberg and Mele[10] suggest phase separation of electrons and holes for $J/t>(J/t)_c$ with $(J/t)_c$ dependent on electron density with $(J/t)_c \sim 3.25$ for $\rho_0=0.75$, the density considered in this paper. In a completely phase-separated state, spin correlations are Heisenberg-like with zero frequency excitations at momentum $q=\pi$. For $2<J/t<(J/t)_c$ Assaad and Würtz find that the equal-time spin correlation function suggests dimer-liquid behavior where bound singlet pairs of spins interact weakly with other pairs. $S_{zz}(q,\omega)$ for immobile nearest-neighbor singlet dimer pairs is given by

$$S_{zz}^{\text{dimer}}(q,\omega) \sim (1-\cos q)\delta(\omega-J) , \tag{5}$$

where the factor $(1-\cos q)$ describes the spin density of a singlet pair and $\omega=J$, the singlet-to-triplet excitation energy, is the only excitation energy observed with $S_{zz}(q,\omega)$, which only probes triplet excited staes (if the ground state is a singlet). Dispersion about the singlet bond breaking energy $\omega=J$ results from interdimer coupling and fluctuations in intradimer binding due to hopping. Finite-size scaling[11] and variational theory[12] suggest that the dispersion extends to zero frequency for large electron filling even for intermediate values of J/t.

II. METHOD

World-line quantum Monte Carlo simulations[5] are used to stochastically evaluate the imaginary-time correlation functions

$$S_{zz}(q,\tau)=\frac{1}{2}\langle e^{H\tau}S_z(q)e^{-H\tau}S_z(-q)\rangle \simeq \frac{1}{2}\sum_R e^{-iqR}\overline{S_z(R,\tau)S_z(R=0,\tau=0)} , \tag{6}$$

$$S_{nn}(q,\tau)=\frac{1}{2}\langle e^{H\tau}n(q)e^{-H\tau}n(-q)\rangle \simeq \frac{1}{2}\sum_R e^{-iqR}\overline{n(R,\tau)n(R=0,\tau=0)} , \tag{7}$$

at a finite set (~ 50) of evenly spaced τ values between 0 and $\beta/2$. The averages indicated on the right-hand sides of Eqs. (6) and (7) are taken over $\sim 10^4$ configurations of the $\sim 10^8$ generated by the world-line Monte Carlo simulation. The statistical errors due to finite Monte Carlo sampling are obtained from the covariance matrix.

$$C(\tau,\tau')=\overline{[S(q,\tau)-\overline{S(q,\tau)}][S(q,\tau')-\overline{S(q,\tau')}]} , \tag{8}$$

which describes the fluctuation of configuration values for $S(q,\tau)$ about their Monte Carlo average $\overline{S(q,\tau)}$. In practice there is a strong correlation between fluctuations at different times τ and τ' and so nondiagonal elements of the covariance matrix are retained. The eigenvalues of $C(\tau,\tau')$, λ_i, describe the error bars σ_i of statistically independent quantities, $S_i(q)$, which are linear combinations of $S(q,\tau)$ at different values of τ. Explicitly

$$\sigma_i=\sqrt{\lambda_i/(N-1)} , \tag{9}$$

where N is the number of binned sets of data which are used in averaging. To test our Monte Carlo algorithm we have compared results from 12-site low-temperature simulations with results of exact diagonalization and find the Monte Carlo results for equal-time correlation functions fall within the error bars of the exact values.

The imaginary-time correlation functions are related to the dynamic structure factors by

$$S(q,\tau)=\frac{1}{2\pi}\int_0^\infty e^{-\omega\tau}(1+e^{-\beta\omega})S(q,\omega)d\omega , \tag{10}$$

or, in terms of the quantities $S_i(q)$,

$$S_i(q)=\int_0^\infty (i|\tau)_\omega S(q,\omega)d\omega , \tag{11}$$

where $(i|\tau)_\omega$ is the scalar product of the ith eigenvector of the covariance matrix and the set of kernels $e^{-\omega\tau}(1+e^{-\beta\omega})/(2\pi)$ for the discrete set of τ values at which $S(q,\tau)$ is evaluated.

The extraction of $S(q,\omega)$ from Eq. (11) is ill-posed for two reasons: (i) there exists an infinite set of functions $S(q,\omega)$ that satisfy Eq. (11) for the discrete set $S_i(q)$, and (ii) the $S_i(q)$ values are only known to within error bars σ_i. The maximum-entropy method provides a technique for producing approximate results[6,13] with the biasing necessary to produce a unique result being toward a predefined "default model" $m(q,\omega)$. To determine a unique approximate result that takes into account stochastic errors, the entropy functional is defined as

$$I[\tilde{S}(q,\omega)]=-\int_0^\infty \tilde{S}(q,\omega)\ln[\tilde{S}(q,\omega)/m(q,\omega)] -\tilde{S}(q,\omega)d\omega , \tag{12}$$

and

$$\chi^2[\tilde{S}(q,\omega)]=\sum_i \frac{(S_i(q)-\int_0^\infty (i/\tau)_\omega \tilde{S}(q,\omega)d\omega)^2}{\sigma_i^2} \tag{13}$$

is the measure of how close the trial function $\tilde{S}(q,\omega)$ comes to reproducing the Monte Carlo results relative to the error bars. The trial function $\tilde{S}(q,\omega)$ which maximizes the functional

$$I-\alpha\chi^2 \tag{14}$$

is chosen as the approximate result for $S(q,\omega)$. The Lagrange multiplier α determines the relative weight given each term in Eq. (14). A large value of α favors a result which produces a close fit to the Monte Carlo results, and a small value of α favors a result similar to the "default model" $m(q,\omega)$ as the maximum of $I[\tilde{S}(q,\omega)]$ occurs for $\tilde{S}(q,\omega)=m(q,\omega)$. While it is not possible to determine a "correct" value of α, it is desirable that the choice for α allows for a good fit to the data, but without overfitting such that spurious, noise-induced features are produced. In this work α is chosen by maximizing a probability distribution as is described by Gubernatis *et al.*[14] When α is chosen this way χ^2 typically has a vaue of $N_\tau-N_\tau/2$, where N_τ is the number of data points. Thus, this procedure is essentially equivalent to fitting the Monte Carlo data to within an error bar on average, while staying as close to the default model $m(q,\omega)$ as possible using information theory to quantify the difference between $S(q,\omega)$ and $m(q,\omega)$.

This dynamical method is most accurate for low frequencies. Equation (10) shows that a feature which is found at a large frequency is quickly suppressed in imaginary time by the factor $e^{-\omega\tau}$. For sufficiently large τ values a high-frequency feature contributes so little to $S(q,\tau)$ that its contribution is swamped by sampling errors. For lower-frequency features, larger values of τ still contain statistically significant weight, so more data points contain statistically significant information.

III. RESULTS FOR $S_{nn}(q,\omega)$

The interpretation of our results for $S_{nn}(q,\omega)$ are aided by exact results for $J=0$. In the thermodynamic limit, the charge dynamics for $J=0$ can be described by spinless noninteracting fermions with the Hamiltonian

$$H=-t\sum_i c_i^\dagger c_{i+1}+c_{i+1}c_i^\dagger$$
$$=\sum_k \varepsilon_k c_k^\dagger c_k,\quad \varepsilon_k=-2t\cos k\ . \tag{15}$$

Thus, in one dimension the t-J model with $J=0$ or the $U/t\to\infty$ Hubbard model with density ρ_0 have the same charge dynamics at the $U/t\to 0$ Hubbard model with density $2\rho_0$.

The analytic result for $S_{nn}(q,\omega)$ for $J/t=0$ is given by

$$S_{nn}(q,\omega)=\frac{\pi}{N}\sum_k f(\varepsilon_k)[1-f(\varepsilon_{k+q})]$$
$$\times\delta(\omega-(\varepsilon_{k+q}-\varepsilon_k))\quad (q\neq 0)\ . \tag{16}$$

This functional form describes "particle-hole" excitations where a fermion is removed from a state with momentum k and placed in an empty state with momentum $k+q$. Figure 1 depicts this process for $q=\pi$. Two excitations that contribute to $S_{nn}(q=\pi,\omega)$ are explicitly noted and demonstrate that $S_{nn}(q=\pi,\omega)$ spans a broad range of frequency. Unlike higher dimensions, one-dimensional particle-hole excitations extend to zero frequency for only two values of momentum $q=\pm 2\pi\rho_0\ (\mathrm{mod}\ 2\pi)$.

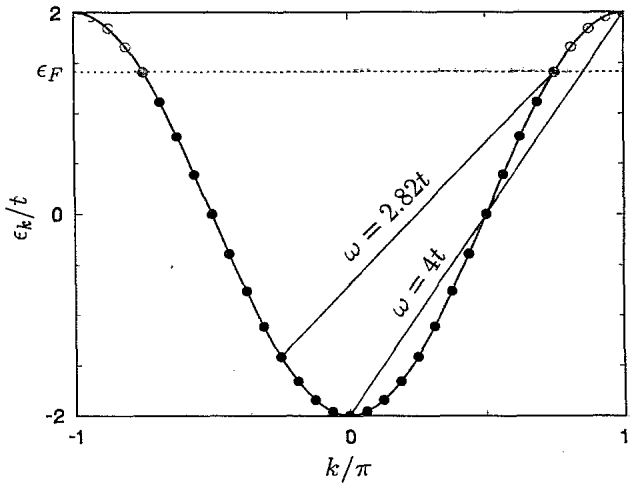

FIG. 1. One-electron states for noninteracting spinless fermions with density $\rho_0=0.75$/site. In the thermodynamic limit the t-J model with $J=0$ is equivalent to a gas of noninteracting spinless fermions. For spinless fermions the excitations described by $S_{nn}(q,\omega)$ correspond to removing a fermion from a state with momentum k and placing it in an empty state with momentum $k+q$ (mod 2π), where ω equal the change in energy. Two excitations which contribute for $q=\pi$ are explicitly shown.

The spinless fermion result for $S_{nn}(q=\pi,\omega)$ for a 64-site system is shown in Fig. 2. The δ functions have been broadened by $0.02t$. Due to the finite size of the system the spectrum is discrete. The greatest weight is found near $\omega=4t$ due to the large density of states near $\varepsilon_k=-2t$ and $2t$ where the bands are flat in Fig. 1. In the thermodynamic limit at $T=0$, the $\omega=4t$ peak becomes a Van Hove singularity diverging as $(4t-\omega)^{-1/2}$.[15] Also,

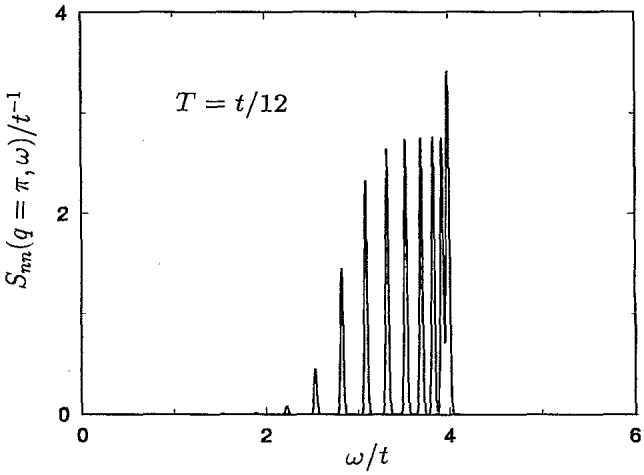

FIG. 2. $S_{nn}(q=\pi,\omega)$ for spinless fermions with 64 sites. The δ function peaks have been broadened by $0.02t$. The strongest contribution comes from the range $\omega=2.8t$ to $4.0t$ as depicted in Fig. 1. The spectrum is discrete due to the finite size of the system. In the thermodynamic limit the cutoff $\omega=4t$ is singular from below at $T=0$. Although the t-J model with $J=0$ is not strictly equivalent to spinless fermions for 64 sites, the overall structure of the spectrum is the same with shifts of the δ functions of order $t/64$.

$\omega=4t$ corresponds to a temperature-independent cutoff in the spectrum; thus the spectrum is very asymmetric.

Figure 3 shows the Monte Carlo $S_{nn}(q=\pi,\tau)$ results that are used in producing an approximate result for $S_{nn}(q=\pi,\omega)$. The data is normalized by

$$\sum_{\sigma}\langle c^{\dagger}_{0,\sigma}c_{1,\sigma}+c^{\dagger}_{1,\sigma}c_{0,\sigma}\rangle=\langle(c^{\dagger}_{0}c_{1}+c^{\dagger}_{1}c_{0})\rangle$$

as suggested by the f-sum rule

$$\frac{1}{\pi}\int_0^{\infty}(1-e^{-\beta\omega})\omega S_{nn}(q,\omega)d\omega = t(1-\cos q)\langle(c^{\dagger}_{0}c_{1}+c^{\dagger}_{1}c_{0})\rangle \ . \quad (17)$$

The exact spinless fermion result and the $J=0$ results are equivalent, demonstrating the smallness of finite-size effects for 64 sites where periodic boundary conditions make the models inequivalent, i.e., having one electron transverse the ring (and causing spin-down and spin-up electrons to exchange positions) does not produce an equivalent configuration. Also, the $J=0$ and $J=2t$ results are nearly the same, suggesting that they describe similar excitations. We return to this point shortly.

Figure 4 shows the eigenvalues of the covariance matrices used in the definition of χ^2 in Eq. (13). The eigenvalues for $J=0$ and $J=2t$ are similar indicating equivalent accuracy for the two cases. Figure 5 shows the default models $m(q=\pi,\omega)$ used in the definition of the entropy in Eq. (12). These default models were chosen to satisfy the sum rules

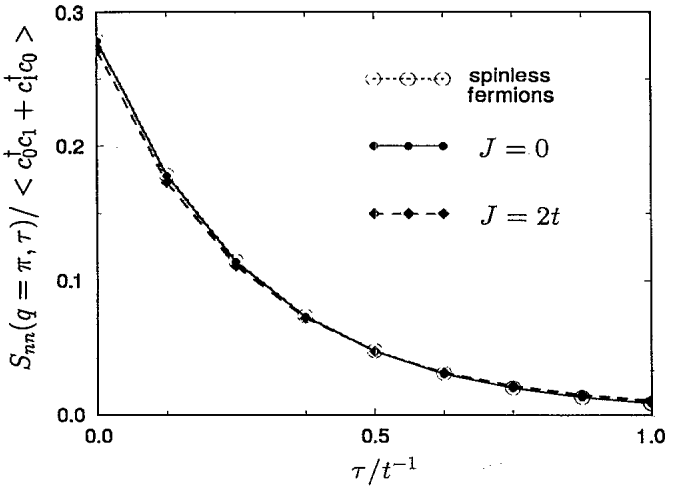

FIG. 3. Imaginary-time correlation function $S_{nn}(q=\pi,\tau)$ normalized by the J-dependent hopping $\langle c^{\dagger}_{0}c_{1}+c^{\dagger}_{1}c_{0}\rangle = \sum_{\sigma}\langle c^{\dagger}_{0,\sigma}c_{1,\sigma}+c^{\dagger}_{1,\sigma}c_{0,\sigma}\rangle$. The spinless fermion result is equivalent to the Monte Carlo result for $J=0$, demonstrating the accuracy of the Monte Carlo results and the smallness of the finite-size effects which make the models inequivalent. Also the $J=2t$ results are similar to those for $J=0$ suggesting that the modes of the distributions $S_{nn}(q=\pi,\omega)$ are close. The rapid decay of this correlation function implies that spectral weight is concentrated at higher frequencies. For $\tau=t^{-1}$ the correlation function for $J=2t$ is approximately 20% larger than for $J=0$, suggesting that the broadening about the mode of $S_{nn}(q=\pi,\omega)$ is larger for $J=2t$ than for $J=0$ because lower-frequency contributions are necessary for large τ correlations.

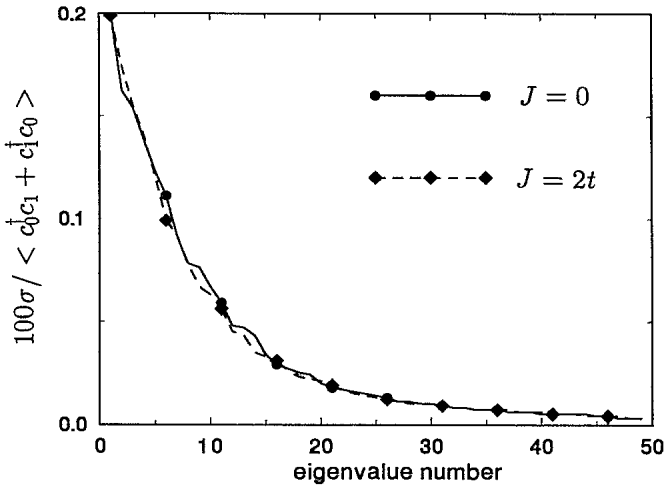

FIG. 4. The error bars obtained for diagonalizing the covariance matrix $C(\tau,\tau')$ and using Eq. (9). The error bars for $J=0$ and $J=2t$ appear to be comparable.

$$\frac{1}{2\pi}\int_0^{\infty}(1+e^{-\beta\omega})m(q,\omega)d\omega=S_{nn}(q,\tau=0) \ , \quad (18)$$

$$\frac{2}{\pi}\int_0^{\infty}(1-e^{-\beta\omega})\omega^{-1}m(q,\omega)d\omega=\chi_{nn}(q) \ , \quad (19)$$

and the f-sum rule of Eq. (17). The right-hand sides are evaluated with Monte Carlo. A unique solution is then chosen by requiring the solution to also maximize

$$-\int_0^{\infty}m(q,\omega)\ln[m(q,\omega)]d\omega \ . \quad (20)$$

Thus the starting point for the calculation uses the available algebraic moments of $S(q,\omega)$ and maximum entropy as has been done for the dynamic structure factor of the xy model.[16] The sum-rule default model is also used for $S_{zz}(q,\omega)$.[7]

Figure 6 shows the results for $S_{nn}(q=\pi,\omega)$. The spin-

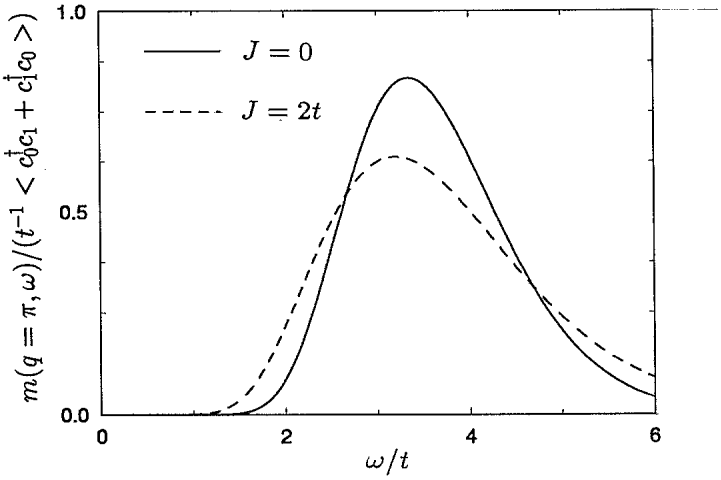

FIG. 5. Default models $m(q=\pi,\omega)$ for $J=0$ and $J=2t$ produced from Eqs. (17)–(20). $S_{nn}(q=\pi,\tau)$ results are used to make improvements to $m(q,\omega)$ to produce a more accurate approximation for $S_{nn}(q=\pi,\omega)$.

less fermion result has been broadened by $0.25t$; this value is chosen so that the maximum of the broadened function has the same magnitude as our $J=0$ result. Figure 6 shows that this method is unable to reproduce the discrete structure expected for a 64-site system as is shown in Fig. 2. Also, the $J=0$ result does not accurately reflect the asymmetry of the spinless fermion result. Nonetheless the maximum-entropy result is an improvement over $m(q,\omega)$ and provides an appropriate description of the spectral weight distribution.

It is interesting that the $J=2t$ result is similar to the result for $J=0$. This is also found for $J=t$ and also for momentum $q=7\pi/8$. This similarity suggests that particle-hole-like excitations dominate for $0<J\leq 2t$ near $q=\pi$ even though single-particle states no longer form eigenstates of the Hamiltonian. The increased width in $S_{nn}(q=\pi,\omega)$ for $J=2t$ could be ascribed to the increased width of the effective single-particle levels, i.e.,

$$S_{nn}(q=\pi,\omega)=\frac{\pi}{N}\int_0^\infty dE\int_0^\infty dE'\sum_k A_k(E)A_{k+q}(E')f(E)[1-f(E')]\delta(w-(E'-E))\ , \tag{21}$$

where $A_k(E)$ is the single-particle spectral function, which is no longer a δ function

$$A_k(E)=\delta(E-\varepsilon_k),\quad \varepsilon_k=-2t\cos k\ , \tag{22}$$

as is found for $J=0$, but now has a finite width. It would be interesting to examine $A_k(E)$ explicitly. von Szczepanski *et al.* have performed numerical studies of finite-size clusters and observe broadening of $A_k(E)$. $A_k(E)$ could also be examined by analytic continuation of the single-particle Green's function

$$G_k(\tau)=-\langle \mathcal{T}_\tau(e^{H\tau}c_k e^{-H\tau}c_k^\dagger)\rangle\ ,$$

but for the t-J model this requires the computationally expansive broken-world-line method. Simulation of the one-dimensional Hubbard model may be more feasible for studying the broadening of $A_k(E)$.[18]

Due to the incompleteness of the Monte Carlo $S_{nn}(q,\tau)$ data, the maximum-entropy method generally produces results broadened with respect to the exact results, as in demonstrated by comparing the $J=0$ and spinless fermion results. It is worth examining whether the broadening found for $J=2t$ is actually required by the Monte Carlo data or is an artifact of this technique. To test this we take the narrow $J=0$ result from Fig. 6 and use this as the default model $m(q=\pi,\omega)$ for $J=2t$. We see in Fig. 7 that $J=2t$ data broadens the $J=0$ result. As stated earlier, the increased broadening is consistent with the imaginary-time data in Fig. 3. There the $J=2t$ correlations are larger than those for $J=0$ for large τ values suggesting the presence of lower-frequency weight for $J=2t$.

The overall spectral intensity,

$$\frac{1}{N\pi}\sum_q\int_{-\infty}^{\infty}S_{nn}(q,\omega)d\omega=\rho_0\ , \tag{23}$$

is a constant for all values of J/t at a fixed filling. We observe that the $q=\pi$ contribution for $J=2t$ is reduced by a factor of $(e_{\text{kin}\ J=2t}e_{\text{kin}\ J=0})\sim 0.9$ relative to $J=0$. Thus spectral weight is shifted to other momenta possibly within some other structure. This is common in many-body systems and often an interaction-induced sharp structure signals a collective mode. For example, in the three-dimensional electron gas without Coulomb interactions $S_{nn}(\mathbf{q},\omega)$ describes the excitation of electron-hole

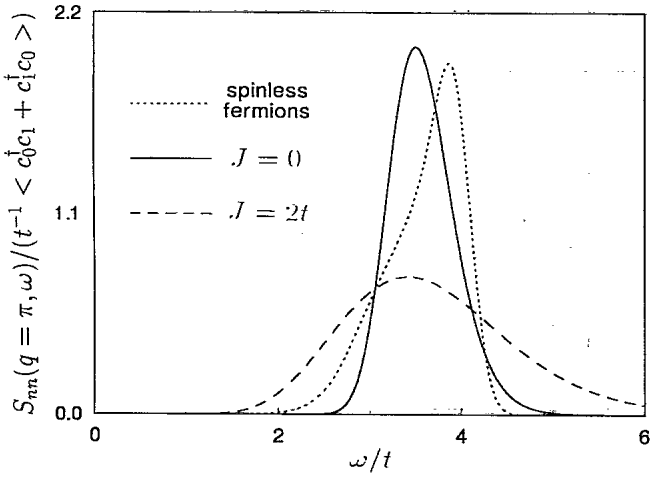

FIG. 6. Maximum-entropy results for $S_{nn}(q=\pi,\omega)$. $J=0$ qualitatively describe the spinless fermion result (which has been broadened with a Gaussian of width $0.25t$), but does not accurately describe the asymmetry. $J=2t$ qualitatively resembles the $J=0$ result, but is substantially broader. If this result is correct, which is considered further in Fig. 7, it suggests that the effective single-particle states near the top and bottom of the band for $J=0$ shown in Fig. 1 are substantially broadened.

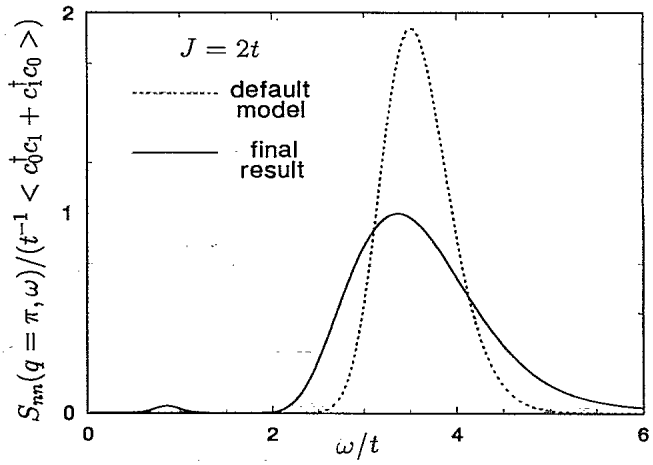

FIG. 7. $S_{nn}(q=\pi,\omega)$ for $J=2t$ using the $J=0$ result as a default model. To test whether the broadening for $J=2t$ is necessary with respect to the more narrow $J=0$ result, we use the $J=0$ result as the default model. Most of the width found in Fig. 6 is restored, confirming that the spectrum for $J=2t$ is indeed substantially broader than for $J=0$.

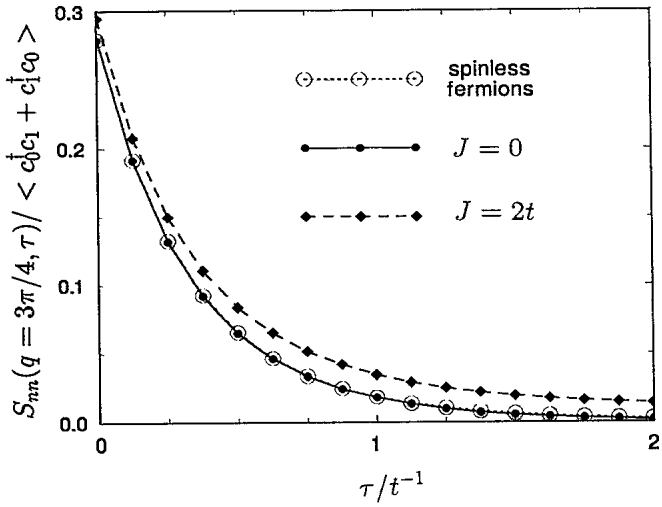

FIG. 8. $S_{nn}(q=3\pi/4, \tau)$. Here the difference between $J=0$ and $J=2t$ is nearly constant for $\tau<2t^{-1}$. This suggests that the high-frequency behavior is similar for $J=0$ and $J=2t$, but $J=2t$ has additional low-frequency weight.

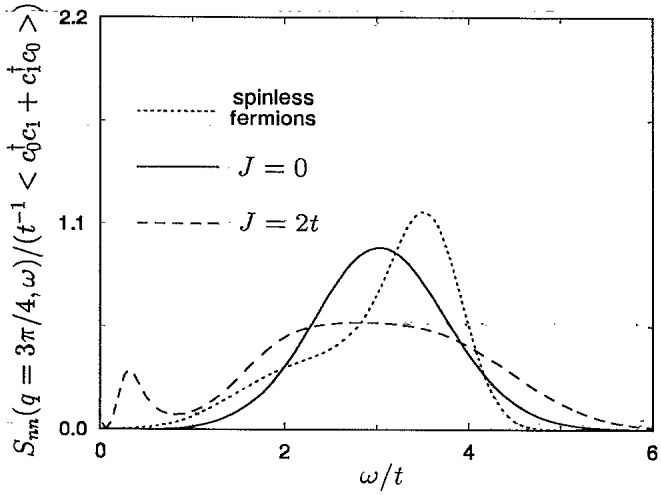

FIG. 9. $S_{nn}(q=3\pi/4, \omega)$. The $J=0$ result again shows the broad particle-hole spectrum, but does not accurately reflect the asymmetry of the spinless fermion result which is broadened here by $0.5t$. The high-frequency piece for $J=2t$ is again broadened relative to $J=0$, but now a feature appears at low frequencies for $J=2t$ that is not observed for $J=0$.

pairs.[17] When the Coulomb interaction is included, $S_{nn}(\mathbf{q},\omega)$ still describes the excitations of electron-hole pairs at large values of $|\mathbf{q}|$, but as $|\mathbf{q}|$ is decreased spectral weight for electron-hole creation is transferred to a plasmon peak.

The $q=3\pi/4$ imaginary-time data displayed in Fig. 8 indeed suggests that a new feature appears at low frequencies for $J=2t$. The difference between the scaled $J=0$ and $J=2t$ data is nearly constant up to $\tau=2t^{-1}$. This constant difference suggests that the high-frequency particle-hole excitations found for $J=0$ have their intensity reduced for $J=2t$ by approximately the same factor (~ 0.9) found for $q=\pi$ and that an excitation appears at a frequency below the particle-hole excitation energies.

The maximum-entropy results for $S_{nn}(q=3\pi/4, \omega)$ are shown in Fig. 9. Again the Monte Carlo result for $J=0$ does not describe the asymmetry of the spinless fermion result (which is broadened by $0.5t$). As was the case for $q=\pi$, the particle-hole-like peak for $J=2t$ is broadened with respect to $J=0$. However, in contrast to $q=\pi$, a low-frequency peak appears near $\omega\sim 0.4t$ The observability of this structure is aided by the lack of particle-hole excitations at low frequencies, which would provide a decay mechanism for the excitation(s) described by this peak. Again, this lack of low-frequency particle-hole intensity is unique to one dimension.

Figure 10 shows the dependence of this feature on J/t. The peak appears for $J=0.5t$, but is most pronounced at $J=t$, even more so than for the $J=2t$ peak displayed in Fig. 9. The spectrum for $J=2.5t$ differs qualitatively from the spectra for $J\leq 2t$ and it is less straightforward to separate particle-hole-like contributions from other features. The position of the peak *decreases as J increases;* the peak is found at $\omega=0.6t$, $0.5t$, and $0.35t$ for $J/t=0.5t$, t, and $2t$, respectively.

Results for $q=\pi/2$ are shown in Fig. 11. For $q=\pi/2$, the change in the spectrum is greater as a function of J/t than for $q=3\pi/4$ and π. We see that the result for $J=t$ shows a sharp low-frequency feature replacing the particle-hole continuum that extends to zero frequency for $J=0$. Figure 12 shows the removal of the low-frequency structure and a qualitative change in the character of the spectrum as J is increased to $2t$ and $2.5t$. Again the additional peak shifts downward from $0.3t$ to $0.2t$ as J increases from t to $2t$. Note that the peak positions are about half of that for $q=3\pi/4$, and thus the excitations being described by the low-frequency peaks are strongly dispersive. No well-defined peak appears for

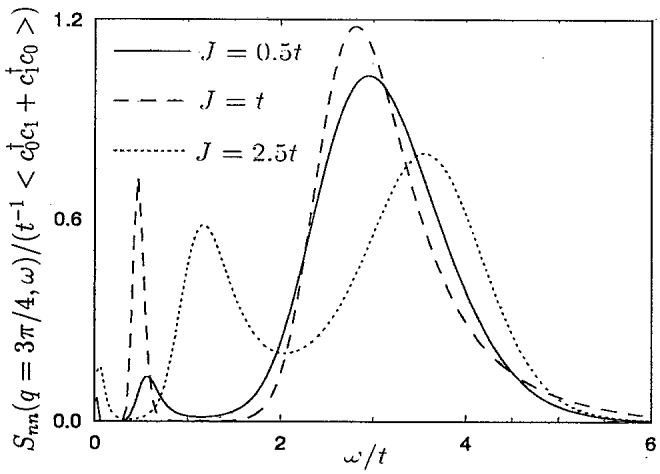

FIG. 10. Dependence of $S_{nn}(q=3\pi/4, \omega)$ on J/t. The $J=0.5t$ result shows evidence of the low-frequency feature at $\omega\sim 0.6t$. For $J=t$ the feature is particularly sharp, suggesting a collective excitation or weakly damped excitation which is not single-particle-like. When J increases to $2.5t$ the character of the spectrum changes indicating that the charge structure of the ground state is different from $J\leq 2t$. The position of the low-frequency peak decreases as J/t increases indicating that the excitation which produces the peak stabilizes with an increasing value of J/t.

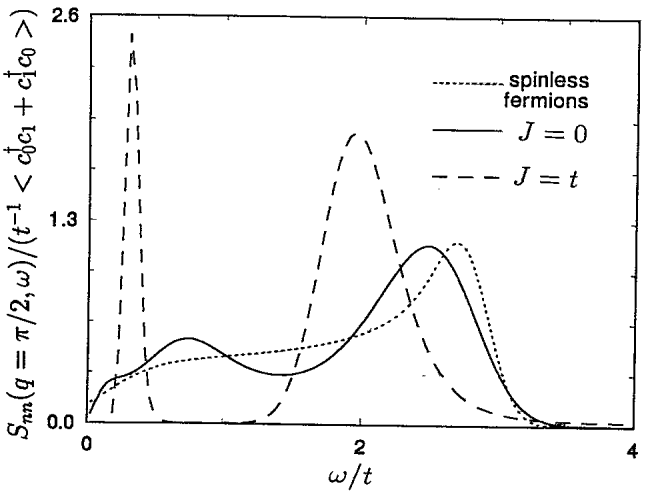

FIG. 11. $S_{nn}(q=\pi/2, \omega)$. The particle-hole spectrum extends to $\omega=0$ for $J=0$, but for $J=t$ the low-frequency spectral weight is concentrated in a single peak at $\omega=0.3t$.

$J=0.5t$ in Fig. 12 due to the large spectral weight for particle-hole excitations found for $J=0$, however, additional structure is emerging.

Figure 13 shows results for $q=\pi/4$. No additional structure appears as J/t is made finite, but the spectrum shifts to lower frequencies as J increases. If these excitations arise from particle-hole-like excitations from near ε_F, this suggests a substantial change in the character of the states formerly found near ε_F. The change in the distribution function n_k from one that is discontinuous at $J=0$ to one that is continuous for finite values of J/t (Refs. 8 and 11) suggests that the low-momentum transfer charge excitations should be strongly affected. Because the broad particle-hole-like continuum in Fig. 13 extends into the range where the sharp low-frequency excitation is found for $q=3\pi/4$ and $\pi/2$, it is of interest to consider other values of the electron density which shift the particle-hole excitations to larger energies allowing a

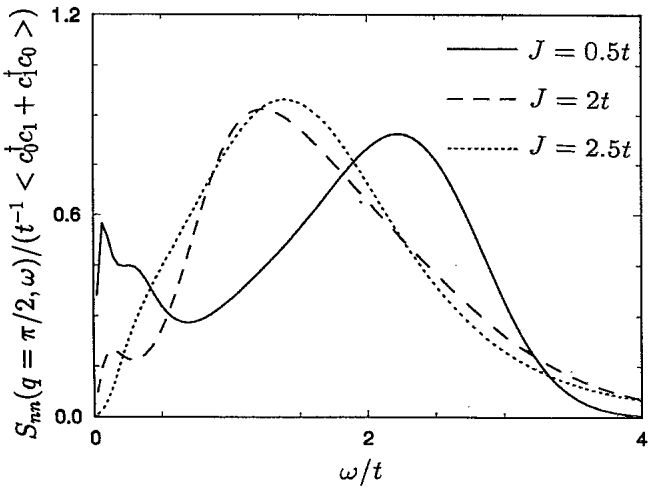

FIG. 12. $S_{nn}(q=\pi/2, \omega)$ as a function of J/t. The sharp peak found for $J=t$ is gradually removed as J/t increases and is no longer distinct at $J=2.5t$. A low-frequency peak appears for $J=0.5t$ imposed on the particle-hole continuum.

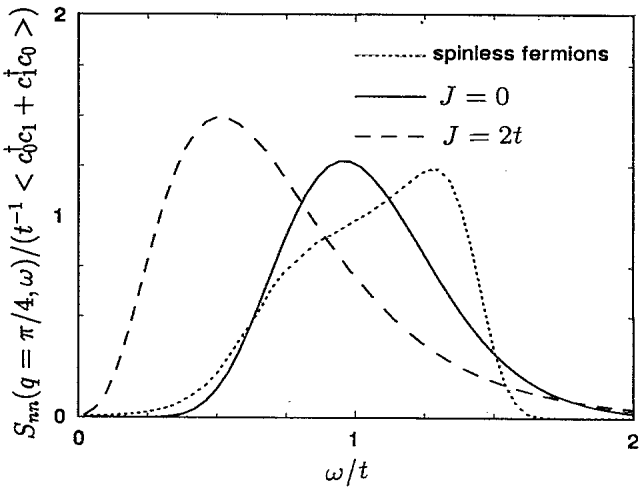

FIG. 13. $S_{nn}(q=\pi/4, \omega)$. The finite values of J/t do not produce an additional low frequency feature for $q=\pi/4$. However, a large shift of the spectral weight to lower frequencies occurs while the spectrum remains broad.

low-frequency feature to appear in $S_{nn}(q=\pi/4, \omega)$.

The electron density $\rho_0=0.5$ produces the largest energies for particle-hole excitations at $J/t=0$. Results for $\rho_0=0.5$ are shown in Fig. 14. As with $\rho_0=0.75$ the particle-hole-like feature broadens and shifts to lower frequencies at J/t increases. Here, though, an additional, but weak, feature does appear at low frequency.

We note that the spinless fermion result in Fig. 14 is only broadened by $0.04t$ in order to obtain the close agreement with our Monte Carlo result. This is a further indication that low-frequency features are accurately described with this method.

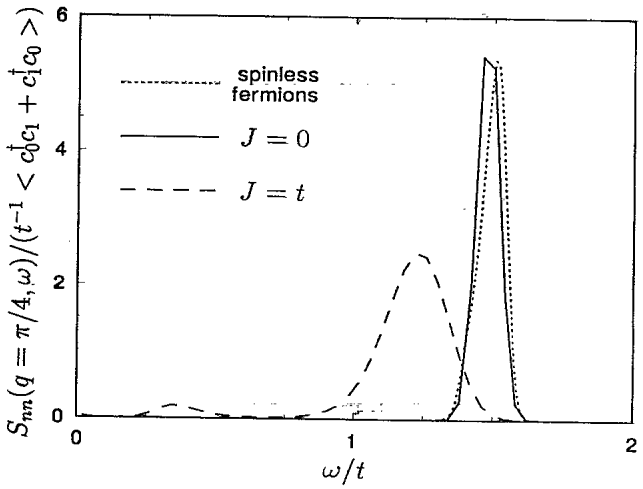

FIG. 14. $S_{nn}(q,\omega)$ electron density $\rho_0=0.5$ and $q=\pi/4$. When the density is lowered to $\rho_0=0.5$ the particle-hole spectral weight is shifted to higher frequencies, distinct from the characteristic energy of the sharp mode. The mode now appears for $J=t$, although it is very weak. Note that the spinless fermion result is broadened by only $0.04t$ in this figure and agrees well with the $J=0$ result. This demonstrates the accuracy of this method at lower frequencies as compared to higher-frequency structures, such as for $q=3\pi/4$, where broadening of the spinless fermion result by as much as $0.5t$ is required.

Because this method does not provide excited-state wave functions, we can only speculate on the nature of the elementary excitations described by the low-frequency structure. The short range of the interaction suggests that the peak describes binding of particles. In the two-electron case, the t-J model shows no binding for $J/t<2$ (independent of dimensionality), as the energy gain from the interaction term is unable to offset the loss of mobility.[19] Binding occurs for $J/t>2$. It seems reasonable that bound pair states exist as excited states for $J/t<2$. Such excited states may be responsible for the low-energy peak observed at these large densities. The decrease in frequency of this peak as J/t increases could then be ascribed to the decrease in energy of two (or more) particle-bound states.

Figures 10 and 12 show that the nature of the charge excitations is qualitatively different for $J=2.5t$ than for $J<t$. This can be ascribed to the bound pair excitations found for $J\leq 2t$ becoming stabilized or contributing to the ground state for $J=2.5t$. For $2<J/t<(J/t)_c$ Assaad and Würtz[9] find that the static spin structure factor is fit by the form $(1-\cos k)$ indicating the presence of bound singlet pairs. Hellberg and Mele[10] find that the Jastrow factor describing their variational wave function changes from one where long-range spin correlations dominate to one where singlet pairing dominates. Monte Carlo[20] and exact diagonalization[11] show the dominance of "superconducting correlations," which describe the prevalence of nearest-neighbor spin-singlet pairs when J/t is increased above 2. The Bethe-ansatz ground-state wave function for $J=2t$ describes a gas of singlet pairs with the binding extending over arbitrarily large distances.[4] All of these exact and numerical results point to the change in the nature of the pair correlations as J/t increases and it seems plausible that the excitation described by the sharp peak in $S_{nn}(q,\omega)$ is related to this change.

Summarizing, results for $S_{nn}(q,\omega)$ show that particle-hole excitations dominate charge spectrum at high frequencies. However, a sharp mode appears at frequencies of order $0.5t$ for finite values of J possibly describing bound singlet pair states. The intensity of the mode is dependent on J/t, q, and the electron filling ρ_0 and is particularly sharp near $J=t$.

IV. RESULTS FOR $S_{zz}(q,\omega)$

Figure 15 shows $S_{zz}(q=\pi,\omega)$ for $J=4t$, $2.5t$, and t. The $J=4t$ result (which is from a simulation with temperature $J/24$, as are all results in this section) corresponds to phase separation at $T=0$ where the spin excitations should be Heisenberg-like. The $J=4t$ result resembles that for the pure Heisenberg model[7] with a broad continuum of excitations extending from $\omega=0$ to $\omega\sim\pi J$. The results obtained for $J=4t$ are affected by ergodicity problems in the Monte Carlo simulation, i.e., the results depend on the initial choice of configuraton and the random number sequence. This is typical of Monte Carlo simulations performed near a phase boundary. We find that ergodicity problems mainly affect the sharpness of the low-frequency peak. This is expected as the thermal excitations introduce low-mobility holes into the Heisenberg chains and, if these holes are static, a gap in the spectrum results due to the finite size of the decoupled spin chains. The holes are not static, but their motion and spatial distribution are precisely what is being poorly described near the phase transition. We consider the ergodicity problem in more detail below along with $q=3\pi/4$ results.

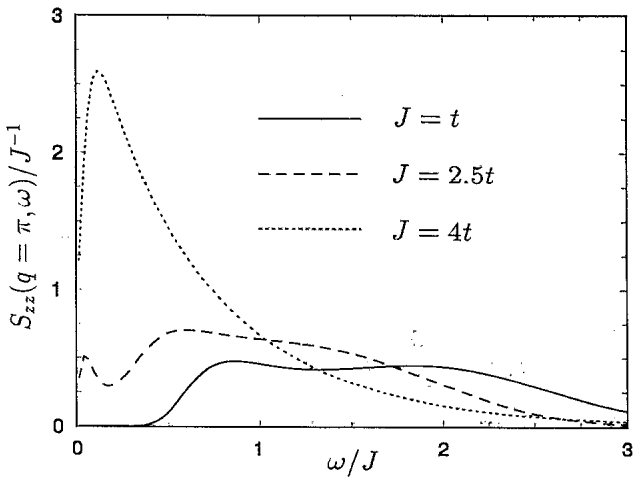

FIG. 15. $S_{zz}(q=\pi,\omega)$. For all values of J/t the spectrum is broad. In the phase-separated state at $J=4t$ we find the Heisenberg-like dynamics with the spectrum extending to low frequency. The $J=t$ spectrum is cut off at a finite frequency as the zero-frequency excitations are found for $q=3\pi/4=2k_F$ for $J\leq 2t$. The $J=2.5t$ spectrum extends to zero frequency demonstrating the absence of a spin gap for this intermediate value of J/t.

For $J=t$, $S_{zz}(q,\omega)$ shows a large gap for $q=\pi(\sim 0.7J)$, but the excitation spectrum remains broad. The size of the gap decreases with respect to J as J/t increases and is approximately $0.3t$ for $J=2t$ (not shown). At $J=2.5t$ there is no longer a discernible gap at $q=\pi$, although the spectral weight remains concentrated at high frequencies.

Figure 16 shows that low-frequency spin excitations are found at $q=2k_F=\pi\rho_0=3\pi/4$ for $J/t\leq 2$ as expected. Three distinct peaks occur for $J=t$ with the lowest-frequency peak at $\omega=0.06t$, a value consistent with being the finite-size gap. Low-frequency spectral weight for $q=3\pi/4$ is reduced as J/t increases. The $J=2.5t$ results have nearly collapsed to the $J=4t$ result except for $\omega<0.5J$ where there is still signficant spectral intensity for $J=2.5t$.

The $J=4t$ results are similar to the Heisenberg results[7] except for the appearance of a low-intensity peak at low frequency. This peak is due to the fluctuations in the phase-separated state and is strongly affected by the ergodicity problems associated with the zero-temperature phase transition. This is demonstrated in Fig. 17 where two results obtained from Monte Carlo simulations differing only in their random-number sequences are shown. The qualitative features are the same, but one result is substantially broadened, especially at low frequencies.

For $J=2.5t$ and for both $q=3\pi/4$ and $q=\pi$, $S_{zz}(q,\omega)$ has excitations extending to zero frequency. As J/t in-

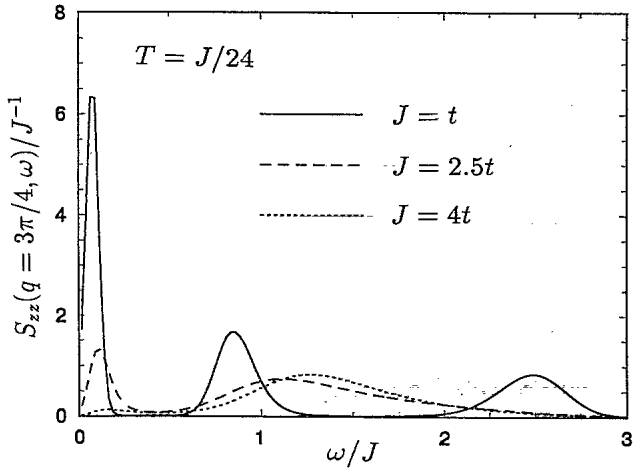

FIG. 16. $S_{zz}(q=3\pi/4, \omega)$. For $J \leq 2t$ low-frequency excitations are found for $q=3\pi/4=\pi\rho_0=2k_F$. The nonzero peak position ($\omega \sim 0.06t$) for $J=t$ is of the order expected for finite-size effects. For $J=4t$ phase separation occurs at $T=0$. For complete phase separation the Heisenberg-like excitations dictate that $q=3\pi/4$ has no spectral weight below $1.1J$. In addition to the maximum-entropy broadening, thermal and quantum fluctuations produce weight below $\omega=1.1t$ for $J=4t$. $J=2.5t$ falls in the crossover regime with most of the spectral intensity at large frequencies, but we still find excitations at low frequencies at $q=3\pi/4$ (and $q=\pi$).

creases this low-frequency weight increases for $q=\pi$ and decreases for $q=3\pi/4$. The opposite is true when J/t decreases from $2.5t$. This suggests that a spin gap is absent for any value of J/t at the filling of $\rho_0=0.75$. It has been suggested, though, that a spin gap may appear at very low densities.[10,11]

The absence of a spin gap for $J=2.5t$ shows that a gas of singlet dimer pairs does not completely represent the nature of the ground state for this large filling. There still remain, though, signatures that these pairs are present in the ground state. The spin excitation energies are concentrated at higher energies, of order $\omega=J$, and the character of the spectrum is weakly momentum dependent (the $q=\pi$ and $q=3\pi/4$ spectra are similar), indicating that the excitations that are probed by $S_{zz}(q,\omega)$ are nearly local.

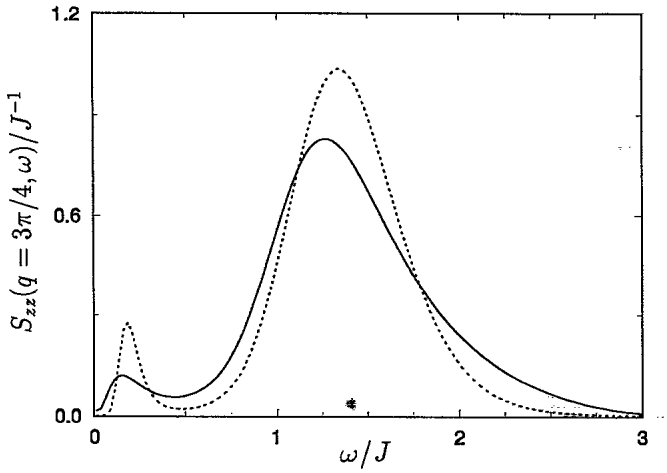

FIG. 17. Comparison of $J=4t$ results for $q=3\pi/4$ for two simulations differing only in their random-number sequence. Because of the proximity of the $T=0$ phase transition, ergodicity effects results for $J=4t$. The same qualitative picture is produced for both simulations with the low-frequency behavior the most poorly converged even though maximum entropy is most accurate for low frequencies.

V. DISCUSSION

These results may be helpful in untangling the excitations described using the Bethe ansatz.[4] The connection between spinon and holon excitations from the Bethe ansatz to the excitations observed with the experimentally relevant quantities $S_{nn}(q,\omega)$ and $S_{zz}(q,\omega)$ is not immediately clear. For example, how do the spinons and holons correspond to what are essentially particle-hole contributions found in Fig. 6? Also, the Bethe-ansatz wave functions or an extension of the variational approach[10] may provide a description of the excitations producing the sharp peaks in $S_{nn}(q,\omega)$.

The one-dimensional Hubbard model is also of interest and may be studied using this method.[21] The identification of the t-J parameters in terms of the Hubbard model parameters $J/t=4t/U$ is rigorous for $U \gg t$, or $J \ll t$, and the sharp charge excitation feature may not survive when the constraint of double occupancy is relaxed. The superconducting pair correlations have been found to be weaker for the Hubbard model than the t-J model,[22] and thus it is questionable whether a sharp additional feature corresponding to pair formation should occur in the Hubbard model. The Hubbard model allows the study of the spectral function $A_k(E)$ (Ref. 23) (but not easily in the world-line method), and it would be interesting to observe the presence of a satellite structure due to the sharp low-energy structure in $S_{nn}(q,\omega)$, if it occurs, in addition to the broadening of the single-particle levels and the addition of the on-site correlation peaks.

It is not straightforward to connect these results to the two-dimensional t-J or Hubbard models. The added dimensionality brings about frustration of hole motion, for example, that is not present in one dimension. It seems possible, though, that the charge spectrum in two dimensions shares some of the features observed here at moderate densities where frustration is not as prevalent. If the sharp charge excitation appears for the one-dimensional Hubbard model, it would be interesting to produce results for $S_{nn}(q,\omega)$ for the two-dimensional Hubbard model at intermediate couplings and low densities to see if the new feature appears with respect to the particle-hole excitations found for $U=0$. If so, it may be worth examining the evolution of this feature as the density is increased towards half filling. If these excitations are pushed to lower energies as the density is increased, it may suggest that they become stabilized near half filling, which is the regime of interest and where quantum Monte Carlo has been least successful.

ACKNOWLEDGMENTS

We gratefully acknowledge useful conversations with N. Bonesteel, J. E. Gubernatis, P. B. Schlottman, and R. N. Silver. This work was supported by NSF Grant No. DMR-8857341 and a grant from the Cray Research Corporation. One of us (D.L.C.) acknowledges support from the A. P. Sloan Research Foundation. J. D. has been supported in part by Ohio State University. Allocation of computer time at the Ohio Supercomputer Corporation is gratefully acknowledged.

*Present address.

[1]P. W. Anderson, Science **235**, 1196 (1987).

[2]F. C. Zhang and T. M. Rice, Phys. Rev. B **37**, 3759 (1988).

[3]M. Ogata and H. Shiba, Phys. Rev. B **41**, 2326 (1990).

[4]P.-A. Bares and G. Blatter, Phys. Rev. Lett. **64** 2567 (1990); P.-A. Bares, G. Blatter, and M. Ogata, Phys. Rev. B **44**, 130 (1991).

[5]M. Suzuki, Commun. Math. Phys. **51**, 183 (1976); M. Barma and B. S Shastry, Phys. Rev. B **18**, 3351 (1978); J. E. Hirsch, D. J. Scalapino, R. L. Sugar, and R. Blankenbecler, *ibid.* **26**, 5033 (1982).

[6]R. N. Silver, D. S. Sivia, and J. E. Gubernatis, in *Quantum Simulations of Condensed Matter Systems,* Proceedings of the International Workshop on Quantum Simulations of Condensed Matter Phenomena, Los Alamos, 1989, edited by J. D. Doll and J. E. Gubernatis (World Scientific, Singapore, 1990), p. 340; R. K. Bryan, Eur. Biophys. J. **18**, 165 (1990).

[7]J. Deisz, M. Jarrell, and D. L. Cox, Phys. Rev. B **42**, 4869 (1990); J. Deisz, Ph.D. thesis, The Ohio State University, 1991.

[8]N. Kawakami and S.-K. Ying, Phys. Rev. Lett. **65**, 2326 (1990).

[9]F. F. Assaad and D. Würtz, Phys. Rev. B **44**, 2681 (1991).

[10]C. Stephen Hellberg and E. J. Mele, Phys. Rev. Lett. **67**, 2080 (1991).

[11]M. Ogata, M. Luchini, S. Sorella, and F. F. Assaad, Phys. Rev. Lett. **66**, 2388 (1991).

[12]M. Imada, in *Quantum Simulations of Condensed Matter Systems* (Ref. 6), p. 127.

[13]S. F. Gull and J. Skilling, IEEE Proc. **F-131**, 646 (1984).

[14]J. E. Gubernatis, M. Jarrell, R. N. Silver, and D. S. Sivia, Phys. Rev. B **44**, 6011 (1991).

[15]S. Katsura, T. Horiguchi, and M. Suzuki, Physica **46**, 67 (1970).

[16]R. Mead and N. Papanicolaou, J. Math. Phys. (N.Y.) **25**, 2404 (1984).

[17]K. J. von Szczepanski, P. Horsch, W. Stephan, and M. Ziegler, Phys. Rev. B **41**, 2017 (1990).

[18]See, for example, B. I. Lundqvist, Phys. Konden. Mater. **6**, 193 (1967).

[19]H.-Q. Lin, Phys. Rev. B **44**, 4674 (1991).

[20]M. Imada, J. Phys. Soc. Jpn. **59**, 4121 (1990).

[21]J. E. Hirsch and D. J. Scalapino, Phys. Rev. B **27**, 7169 (1983).

[22]M. Imada and Y. Hatsugai, J. Phys. Soc. Jpn. **58**, 3752 (1989).

[23]S. R. White, Phys. Rev. B **44**, 4670 (1991).